Systematic Structural Characterization of the High-Temperature Behavior of Nearly Stoichiometric Silicon Oxycarbide Glasses

H. Bréquel,[†] J. Parmentier,[‡] S. Walter,[‡] R. Badheka,[§] G. Trimmel,[§] S. Masse,[§] J. Latournerie,[||] P. Dempsey,[||] C. Turquat,[⊥] A. Desmartin-Chomel,[#] L. Le Neindre-Prum,[&] U. A. Jayasooriya,[#] D. Hourlier,[||] H.-J. Kleebe,[⊥] G. D. Sorarù,[‡] S. Enzo,[†] and F. Babonneau*[,§]

Dipartimento di Chimica, Universita di Sassari, Italy, Dipartimento di Ingegneria dei Materiali, Universita di Trento, Italy, Chimie de la Matière Condensée, UPMC, Paris, France, Laboratoire de Céramiques Nouvelles, Université de Limoges, France, Institute of Materials Research, University of Bayreuth, Germany, School of Chemical Sciences, University of East Anglia, U.K., and belChem, Brand-Erbisdorf, Germany

Received January 27, 2004. Revised Manuscript Received April 21, 2004

Three silicon oxycarbide glasses (SiCO) with increasing C content were obtained through pyrolysis in inert atmosphere at 1000 °C of sol−gel derived siloxane networks containing $Si-CH_3$ and Si−H bonds. The glasses were further annealed at 1200, 1400, and 1500 °C to follow their evolution at high temperature. Quantitative information concerning the structure of glasses before and after annealing at high temperature was collected with a wide range of techniques (some of them used for the first time in this field) with the aim of probing the following: (i) the short-range order and chemical composition (^{29}Si and ^{1}H MAS NMR, RDF derived from X-ray and neutron scattering, inelastic neutron scattering, FT-IR, and elemental analysis), and (ii) the long-range order (X-ray and neutron diffraction) and microstructural features (HR-TEM combined with electron diffraction, Raman, porosity, and surface area measurements). This extensive collection of data, carried out *on the same set of specimens*, provided detailed and sound structural information on nearly-stoichiometric SiCO glasses and their high-temperature behavior.

I. Introduction

In the last twenty years, polymer pyrolysis for preparing glasses and ceramics has been developed as an alternative to the classical powder processing route[1]. The main driving force is the need to produce high-purity materials with tailored micro/nanostructure and to process at low temperature components with complex shapes, such as fibers, coatings, or matrixes for CMCs. Many efforts have been devoted to the preparation of nitrides and carbides in the Si−C, Si−C−N, Si−B−C−N, B−N, and B−C−N systems.[2,3] Alternatives to non-oxide systems could be oxygen-based silicon oxycarbide (SiCO) glasses which display enhanced mechanical, thermal, and chemical properties compared to those of the pure SiO_2 glass.[4−6] SiCO glasses can be easily prepared through pyrolysis at 1000 °C in inert atmosphere of cross-linked siloxane networks containing Si−R bonds (R = H, CH_3, CH_2CH_3, C_6H_5, ...).[7−9] These preceramic networks can be produced from molecular organosilanes using sol−gel process,[7,8,10−15] from commercially available polysiloxanes,[9,16−19] or from modified

* To whom correspondence should be addressed. Laboratoire Chimie de la Matière Condensée, Université Paris 6 T54 C54/55 E5, 4 place Jussieu, 75252 Paris Cedex 05 France. Tel: (33) 1 44 27 41 35. Fax: (33) 1 44 27 47 69. E-mail: fb@ccr.jussieu.fr.

[†] Universita di Sassari.

[‡] Universita di Trento.

[§] Chimie de la Matière Condensée, UPMC.

[||] Université de Limoges.

[⊥] University of Bayreuth.

[#] University of East Anglia.

[&] belChem.

(1) Riedel, R. Advanced Ceramics from Inorganic Polymers. In *Processing of Ceramics, Part II*; Brook, R. J., Ed.; Materials Science and Technology, Vol. 17B; VCH: Weinheim, Germany, 1996; pp 1−50.

(2) Laine, R. M.; Babonneau, F. *Chem. Mater.* **1993**, *5*, 260.

(3) See papers in special issue on Ultrahigh-Temperature Ceramics. *J. Am. Ceram. Soc.* **2001**, *10*, 84. High Performance Non-Oxide Ceramics, Vols. 101 and 102;Jansen, M., Ed.; Structure and Bonding Series; Springer: Berlin, 2002.

(4) Sorarù, G. D.; Dallapiccola, E.; D'Andrea, G. *J. Am. Ceram. Soc.* **1996**, *79*, 2074.

(5) Rouxel, T.; Massouras, G.; Sorarù, G. D. *J. Sol-Gel Sci. Technol.* **1999**, *14*, 83.

(6) Sorarú, G. D.; Modena, S.; Guadagnino, E.; Colombo, P.; Egan, J.; Pantano, C. *J. Am. Ceram. Soc.* **2002**, *85*, 1529.

(7) Babonneau, F.; Thorne, K.; Mackenzie, J. D. *Chem. Mater.* **1989**, *1*, 554.

(8) Zhang, H.; Pantano, C. G. *J. Am. Ceram. Soc.* **1990**, *73*, 958.

(9) (a) Renlund, G. M.; Prochazka, S.; Doremus, R. H. *J. Mater. Res.* **1991**, *6*, 2716. (b) Renlund, G. M.; Prochazka, S.; Doremus, R. H. *J. Mater. Res.* **1991**, *6*, 2723.

(10) Belot, V.; Corriu, R. J. P.; Leclercq, D.; Mutin, P. H.; Vioux, A. *J. Non-Cryst. Solids* **1994**, *176*, 33.

(11) Corriu, R. J. P.; Leclercq, D.; Mutin, P. H.; Vioux, A. *J. Mater. Sci.* **1995**, *30*, 2313.

(12) Bois, L.; Maquet, J.; Babonneau, F.; Bahloul, D. *Chem. Mater.* **1995**, *7*, 975.

(13) Mutin, P. H. *J. Sol-Gel Sci. Technol.* **1999**, *14*, 27.

(14) Kamiya, K.; Katayama, A.; Suzuki, H.; Nishida, K.; Hashimoto, T.; Matsuoka, J.; Nasu, H. *J. Sol-Gel Sci. Technol.* **1999**, *14*, 95.

(15) Takamura, N.; Taguchi, K.; Gunji, T.; Abe, Y. *J. Sol-Gel Sci. Technol.* **1999**, *16*, 227.

(16) Wilson, A. M.; Zank, G.; Eguchi, K.; Xing, W.; Yates, B.; Dahn, J. R. *Chem. Mater.* **1997**, *9*, 1601.

10.1021/cm049847a CCC: $27.50
Published on Web 05/29/2004

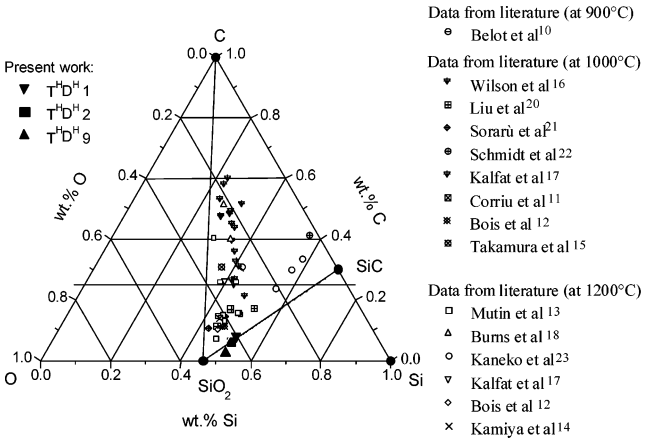

Figure 1. Si−C−O phase diagram showing the binary stable thermodynamic phases (SiO_2 and SiC), and the composition of the stoichiometric silicon oxycarbide glasses ($SiC_xO_{2(1-x)}$). Compositions of SiCO glasses reported in the literature have also been plotted on this diagram.

polycarbosilanes.[20−23] A large range of compositions has thus been obtained that can be represented in a ternary Si−C−O phase diagram (Figure 1). In this diagram, the line connecting SiC and SiO_2 phases represents compositions in which all C atoms are bonded to silicon and no excess or free C is present. The general stoichiometry on the SiC−SiO_2 line is $SiC_xO_{2(1-x)}$. It can be useful to rewrite it as xSiC + $(1 - x)SiO_2$ to realize that the x value in the silicon oxycarbide formula is a direct measure of the relative proportion between Si−C and Si−O bonds present in the glass network. However, SiCO glasses studied so far (Figure 1) usually contain excess C, their composition falls inside the C−SiO_2−SiC triangle, and must be expressed as $SiC_xO_{2(1-x)}$ + yC_{free}.

The problem of controlling the composition of the resulting oxycarbide phase, i.e., the x value of substituted C, and the amount y of the free carbon phase has been addressed in the literature.[24] This study suggests that, as a first approximation, the amount of carbon bonded to silicon in the oxycarbide structure is related to the oxygen content in the precursor gel $(O/Si)_{gel}$. This model is thus a convenient guide to choosing different polysiloxanes to prepare glasses with a large compositional range. In this respect, the sol−gel approach offers the possibility of producing polysiloxanes with tailored composition by an appropriate choice of the starting monomeric silanes.

However, despite the large number of papers that have been published in the last 10 years on the synthesis and characterization of silicon oxycarbide glasses[25] and in the related field of polymer-derived ceramics,[3] fundamental scientific issues still need to be addressed, such as (i) the influence of the synthesis procedure and thermal processing on the final glass composition and structure, and (ii) the high-temperature ($T \geq 1000$ °C) crystallization and/or phase-separation process. One reason for this situation is certainly due to the lack, among the various research groups, of a common processing protocol, which prevents an easy comparison of the large amount of experimental findings available in the literature. Indeed, because of the sensitivity of these materials to many different synthesis and processing parameters, even when dealing with silicon oxycarbide glasses produced from a polysiloxane precursor with the same nominal chemical composition, different experimental results and high-temperature behaviors were reported.[26] Moreover, polymer-derived glasses usually possess very complex micro/nanostructures, with amorphous and nanocrystalline phases that coexist. A detailed characterization of the structure of these samples is thus necessary and requires information from many different techniques.

The objective of this paper was to conduct the structural characterization of nearly stoichiometric silicon oxycarbide glasses, with compositions close to the tie-line between SiC and SiO_2, and to study their crystallization behavior under inert atmosphere between 1000 and 1500 °C. According to previously published data,[27] such glasses can be obtained from sol−gel-derived polysiloxanes containing various amounts of Si−H and $Si-CH_3$ groups. In the present work, three gels, called T^HD^HX ($X = T^H/D^H = 1, 2, 9$) have been prepared from a mixture of triethoxysilane and methyldiethoxysilane in 1:1, 2:1, and 9:1 molar ratios. They have been pyrolyzed at 1000 °C to give SiCO glasses, which were found to be, respectively (see Figure 1): (i) inside the SiO_2−SiC−C triangle, suggesting the presence of an excess of C (T^HD^H1), (ii) close to the stoichiometric SiC−SiO_2 line, indicating the formation of an almost pure silicon oxycarbide glass (T^HD^H2), and (iii) inside the SiO_2−SiC−Si triangle, suggesting the presence of an excess of Si (T^HD^H9). This illustrates the reliability of the adopted method for controlling the composition of the oxycarbide phase through the proper choice of the gel composition.[24]

The SiCO glasses produced at 1000 °C were finally heated to 1500 °C under well-defined conditions (heating rate, atmosphere, crucible, furnace, amount of gel treated in each run, and powder size) to follow their HT structural evolution and to assess the resistance of the glassy material toward crystallization. To avoid the above-mentioned problems related to the sensitivity of these materials to the processing conditions, *the same samples* have been characterized by a wide range of techniques to probe short- as well as long-range order and to characterize the *nano*- as well as *micro*-structure. For the first time in this field, experimental conditions for each of these complementary techniques (^{29}Si and ^{1}H solid-state NMR, FTIR, Raman spectroscopy, X-ray and neutron diffraction, inelastic neutron scattering,

(17) Kalfat, R.; Babonneau, F.; Gharbi, N.; Zarrouk, H. *J. Mater. Chem.* **1996**, *6*, 1673.
(18) Burns, G. T.; Taylor, R. B.; Xu, Y.; Zangvil, A.; Zank, G. A. *Chem. Mater.* **1992**, *4*, 1313.
(19) Berndt, F.; Jahn, P.; Rendtel, A.; Motz, G.; Ziegler, G. *Euro Ceramics VII, PT 1−3, Key Eng. Mater.* **2002**, *206*, 1927.
(20) Liu, Q.; Shi, W.; Babonneau, F.; Interrante, L. V. *Chem. Mater.* **1997**, *9*, 2434.
(21) Sorarù, G. D.; Liu, Q.; Interrante, L. V.; Apple, T. *Chem. Mater.* **1998**, *10*, 4047.
(22) Schmidt, W. R.; Interrante, L. V.; Doremus, R. H.; Trout, T. K.; Marchetti, P. S.; Maciel, G. E. *Chem. Mater.* **1991**, *3*, 257.
(23) Kaneko, K.; Kakimoto, K. I. *J. Non-Cryst. Solids* **2000**, *270*, 181.
(24) Sorarù, G. D. *J. Sol-Gel Sci. Technol.* **1994**, *2*, 843.
(25) See papers in special issue on Silicon Oxycarbide Glasses by Chemical Route. *J. Sol-Gel Sci. Technol.* **1999**, *14* [1].
(26) Parmentier, J.; Sorarù, G. D.; Babonneau, F. *J. Eur. Ceram. Soc.* **2001**, *21*, 817.
(27) Sorarù, G. D.; D'Andrea, G.; Campostrini, R.; Babonneau, F. *J. Mater. Chem.* **1995**, *5*, 1363.

transmission electron microscopy, porosity, and density measurements) have been optimized to extract the maximum of structural information on the various SiCO glasses and their phase separation/crystallization behavior at high temperature.

II. Experimental Section

II.1. Synthesis. Methyldiethoxysilane $HCH_3Si(OEt)_2$ (MDES) and triethoxysilane $HSi(OEt)_3$ (TREOS) precursors (ABCR, Karlsruhe, Germany) were used as received. Three gels called T^HD^HX with $X = 1$, 2, and 9 were prepared with TREOS/MDES molar ratios of 1, 2, and 9 according to the following procedure. The precursors were mixed with ethanol (EtOH/Si = 2) and then co-hydrolyzed with a stoichiometric amount of water at pH = 4.5 (H_2O/OEt = 1). The solution was left under vigorous stirring for 15 min, and then poured into plastic test tubes, which were left open for gelation at room temperature. Then the samples were placed in a drying oven, and the temperature was increased up to 120 °C by steps of 20 °C every 2 days. The resulting dried gels were then ground and sieved. For heat treatments, the coarse fraction of powder whose particle size was in the range 100−350 μm was used to characterize the structural evolution of samples in a manner that could be representative of bulk more than thin components such as fibers or films. The SiCO glasses were obtained by pyrolyzing batches of 2 g of powder in a silica crucible at 1000 °C for 1 h under flowing argon (100 cm^3/min) and with a heating rate of 10 °C/min (silica tubular furnace ROK/A Heraeus). Then the resulting glasses were heat treated, using a graphite furnace, at 1200, 1400, or 1500 °C under Ar (100 cm^3/min) in a carbon crucible for 1 h at a heating rate of 10 °C/min (Astro Furnace, Thermal Technology Inc.)

II.2. Experimental Techniques. Quantitative elemental analysis (EA) of the samples for silicon, carbon, and hydrogen were performed at the Service d'Analyse Elémentaire du CNRS (Vernaison, France). The oxygen amount was determined by difference.

Thermogravimetric analysis (TGA) was carried out by loading 400 mg of sample in alumina crucibles under He (N60) atmosphere (25 cm^3/min flow rate) with a Netzsch STA 409 instrument. The heating rate used was 10 °C/min with a final isothermal holding at 1500 °C for 1 h. The gases produced during pyrolysis were identified in a continuous process using a quadrupole mass spectrometer (MS) (Quadrex 200, Leybold Heraeus, Les Ulis, France, 70 eV, electron impact ionization).

The sample densities were measured using a He-pycnometer (Multivolume Pycnometer 1305, Micromeritics). N_2 adsorption−desorption isotherms were recorded at 77 K on an ASAP 2010 Micromeritics apparatus at relative pressures P/P_0 in the range of $0.05 \leq P/P_0 \leq 0.99$.

High-resolution transmission electron microscopy (HRTEM) experiments were performed with a Philips CM20 field emission gun electron microscope operated at an accelerating voltage of 200 kV (wavelength $\lambda = 0.0251$ Å) using a double-tilt sample holder. Both imaging and diffraction modes were employed for specimen characterization. The sample specimens were prepared through dispersion of powders on copper grids covered with holey-carbon films.

For the diffraction experiments, the powdered specimens were pressed to form a pellet 2−3 mm thick and ca. 14 mm in diameter. X-ray diffraction (XRD) patterns were collected with a Bragg−Brentano powder diffractometer equipped with a graphite monochromator and using Cu Kα radiation (λ = 1.54178 Å) and Mo Kα radiation ($\lambda = 0.7107$ Å) for the usual XRD analysis and the RDF calculations, respectively. The data collection range was from $2\theta = 6$ to 145°. The values of $S_{max} = 4\pi \cdot \sin\theta/\lambda$ achieved with the two radiations employed are 7.6 and 16.8 $Å^{-1}$, respectively. For fully amorphous specimens the raw data handling was performed in a homemade program including (i) usual corrections; (ii) normalization process by the method of Krogh-Moe-Norman;[28,29] (iii) calculation of the reduced scattering intensity I(S) and the interference function S·I(S); and (iv) Fourier transform procedure leading to the reduced radial distribution function (RDF).

The neutron diffraction patterns were collected at the ISIS−RAL facility in Chilton (UK), using the new GEneral Materials diffractometer (GEM) instrument devised for the determination of the structure factor in amorphous and semicrystalline compounds.[30] The instrument makes use of 6 detectors to achieve high-Q resolution and high counting rate simultaneously with high-peak resolution in the presence of crystalline phases.

The evaluation of crystalline phases developed from the amorphous matrix was also carried out both on X-ray and neutron patterns by using the MAUD program.[31] Basically, this program is able to treat quantitatively the structure factor of the amorphous phase, on the grounds of a "nano-paracrystalline" model developed by Le Bail[32] for amorphous silica, from relative comparison with other crystalline phases that may be present in the specimens. The procedure does not need any internal standard. This approach was calibrated successfully in the case of X-ray patterns[33] and, to the best of our knowledge, it is applied here for the first time in the case of neutron diffraction data of semicrystalline substances.

Raman spectra (4000−250 cm^{-1}) were recorded using a Jobin-Yvon 500M spectrophotometer equipped with a CCD detector. The laser excitation used 16 mW at the sample from a Liconix He−Cd laser at 441.6 nm, with a spectral resolution better than 4 cm^{-1}.

INS spectra were recorded using the inelastic spectrometer TOSCA at the spallation neutron source (ISIS) of the Rutherford Appleton Laboratory, UK. TOSCA offers high resolution, ~2% $\Delta E/E$ between 16 and 4000 cm^{-1}. Samples (~4 g) were contained in thin aluminum foil at ca. 25 K during spectral accumulation.

Solid state ^{29}Si magic angle spinning nuclear magnetic resonance (MAS NMR) spectra were collected using two spectrometers (MSL300 and MSL400, Bruker) operating at frequencies of 59.63 and 79.49 MHz, respectively, and equipped with Bruker CP/MAS probes. Samples were finely ground and packed into ZrO_2 rotors (7-mm diam) and spun (4 kHz). The saturation recovery experiments with variable relaxation delays ranging from 1 to 60 s were employed to measure the spin−lattice relaxation times (T_1) for silicon species. For the single-pulse experiments, FIDs were acquired with 90° pulse width and recycle delays of 100 s for the 1000 °C heated samples and of 150 s for the 1200−1500 °C heated samples, a spectral width of 30 kHz, 4096 data points in the time domain; the number of scans depends on the sample (usually around 1000−1200). All chemical shifts (δ) were referenced to tetramethylsilane (TMS; $\delta = 0$). The FID data were processed using WinNMR-1D software, and a line broadening of 50 Hz was applied before Fourier transformation. The experimental spectra were simulated using WinFit modeling software.[34] Solid-state ^1H MAS NMR spectra were collected using a Bruker AVANCE spectrometer operating at the frequency of 600.13 MHz and equipped with a 2.5-mm Bruker CP-MAS probehead. Samples were finely ground and packed into ZrO_2 rotors with Vespel caps and spun to 32 kHz. Each spectrum was recorded with a recycle delay of 5 s, a 250-kHz sweep width, 2048 data points in the time domain, and 8 acquisition scans.

(28) Krogh-Moe, J. *Acta Crystallogr.* **1956**, *9*, 951.
(29) Norman, N. *Acta Crystallogr.* **1957**, *10*, 370.
(30) Hannon, A. C. Neutron Diffraction, Instrumentation. In *Encyclopedia of Spectroscopy and Spectrometry* Lindon, J., Tranter, G., Holmes, J., Eds.; Academic Press: London, 2000; Vol. 2, pp 1479−1492.
(31) Lutterotti, L.; Gialanella, S. *Acta Mater.* **1998**, *46*, 101.
(32) Le Bail, A. *J. Non-Cryst. Solids* **1995**, *183*, 39.
(33) Lutterotti, L.; Ceccato, R.; Dal Maschio, R.; Pagani, E. *Mater. Sci. Forum.* **1998**, *278−281*, 93.
(34) Massiot, D.; Fayon, F.; Capron, M.; King, I.; Le Calvé, S.; Alonso, B.; Durand, J. O.; Bujoli, B.; Gan, Z.; Hoatson, G. *Magn. Reson. Chem.* **2002**, *40*, 70. (http://crmht-europe.cnrs-orleans.fr).

Table 1. Elemental Analysis and Char Yield Measured on Powdered Samples after Pyrolysis for 1 Hour at a Given Temperature

T^HD^H ratio	thermal treatment	weight%				molar ratio			char yield	
		Si	C	O	H	C/Si	O/Si	H/Si	pyrolysis	TGA
	gel	48.69	11.08	35.88	4.35	0.53	1.29	2.49		
	1000°C	50.82	8.37	39.83	0.98	0.39	1.38	0.54	87.6	87.3
1	1200°C	51.25	8.31	40.44	<0.03	0.38	1.39	<0.03	86.6	87.1
	1400°C	51.95	7.66	40.40	<0.03	0.35	1.37	<0.03	82.8	86.0
	1500°C	51.61	7.29	41.10	<0.03	0.33	1.40	<0.03	80.5	77.7
	gel	51.24	7.75	37.46	3.55	0.35	1.28	1.93		
	1000°C	50.57	6.49	42.94	<0.03	0.30	1.49	<0.03	92.9	91.4
2	1200°C	50.90	5.80	43.30	<0.03	0.27	1.49	<0.03	90.5	91.2
	1400°C	52.33	5.76	41.91	<0.03	0.26	1.41	<0.03	89.4	89.1
	1500°C	52.11	5.78	42.11	<0.03	0.26	1.42	<0.03	87.5	87.1
	gel	50.19	5.10	42.19	2.52	0.24	1.48	1.40		
	1000°C	50.53	3.02	46.45	<0.03	0.14	1.61	<0.03	94.5	93.8
9	1200°C	51.76	2.64	45.60	<0.03	0.12	1.55	<0.03	94.0	93.9
	1400°C	51.90	2.96	45.14	<0.03	0.13	1.53	<0.03	94.0	93.9
	1500°C	51.51	2.50	45.99	<0.03	0.11	1.57	<0.03	91.9	94.3

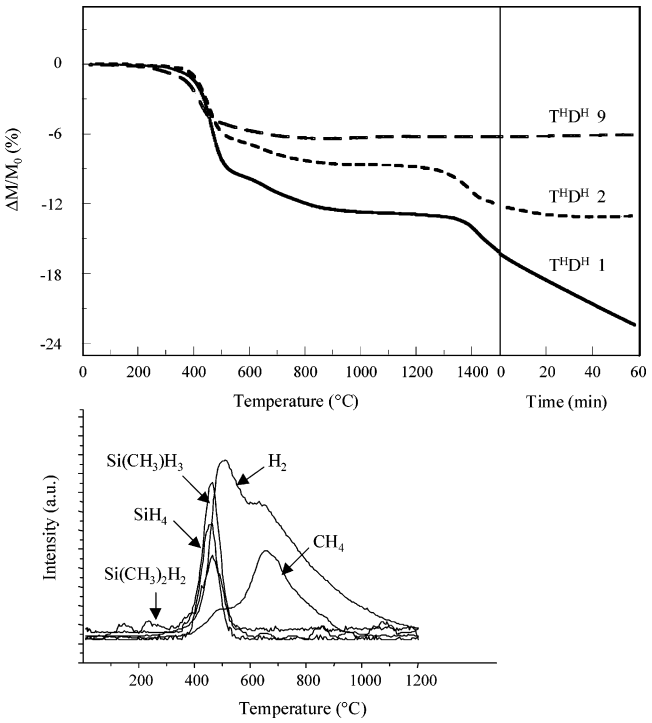

Figure 2. TG profiles of T^HD^H1, 2, and 9 gels pyrolyzed at 10 °C/min, under helium (25 cm^3/min flow rate) up to 1500 °C with an isothermal holding time of 1 h (top) and corresponding MS profile of T^HD^H2 (bottom).

III. Results

III.1. Gel and Glass Synthesis. The composition of the three gels has been investigated by elemental analysis (Table 1), and by ^{29}Si and ^{13}C MAS NMR. As explained in a previous paper,[27] we have verified by ^{29}Si NMR that the Si−H bonds had not been hydrolyzed during synthesis, and that the extent of network condensation is very high. The elemental analysis (C/Si ratio) and ^{13}C MAS NMR results suggest only some residual alkoxy groups in the T^HD^H9 gel. A more detailed structural analysis of such gels can be found in the literature.[27]

The thermal behavior of each T^HD^H gel was then followed by TG/MS (Figure 2).[35] A small weight loss (1−2 wt %) occurs from ambient temperature to 400 °C, essentially due to evaporation of solvent and/or completion of condensation reactions with evolution of H_2O and EtOH. The temperature range between 400 and 600 °C is instead characterized by a more consistent weight loss (from 3−10 wt %) involving Si-containing volatile species: this corresponds to redistribution reactions between Si−O and Si−C bonds.[36] Then, from 600 to 1000 °C, the weight losses associated mainly with H_2 and CH_4 evolutions are due to the polymer-to-glass transformation. Above 1000 and until 1300 °C, no weight losses are observed. Then up to 1500 °C, T^HD^H1 and T^HD^H2 samples show an appreciable weight loss (∼3%) which is not the case for the T^HD^H9 specimen. This behavior is mirrored in the corresponding MS profiles by the evolution of carbon monoxide, observed only for T^HD^H1 and T^HD^H2 samples, the high-C content products of our series, related to carbothermal reduction reactions that will be discussed later.

According to these results, we can assume that the conversion of the polysiloxane into an inorganic network is achieved at 1000 °C. In the following study, we will thus use a heat treatment at this temperature to prepare the SiCO glasses. They will then be annealed at 1200, 1400, and 1500 °C to study their thermal behavior.

III.2. Elemental Analysis. The EA results for the three series of samples (T^HD^H1, T^HD^H2, and T^HD^H9) are reported in Table 1. The chemical compositions of the glass samples (1000 °C) are in agreement with previously published data,[37] with respective C/Si molar ratios of 0.14, 0.30, and 0.39 for T^HD^H9, 2, and 1. These values have been reported in the ternary Si−C−O diagram presented in Figure 1.

The chemical compositions of the samples do not change too much from 1000 to 1500 °C, despite the observation of weight losses. This behavior is directly related to reactions occurring at high temperature between SiO_2-rich phase and the free C. The overall reaction usually proposed for carbothermal process is

$$SiO_2(s) + 3\,C(s) \rightarrow SiC(s) + 2\,CO(g) \qquad (1)$$

(35) Gualandris, V.; Hourlier-Bahloul, D.; Babonneau, F. *J. Sol-Gel Sci. Technol.* **1999**, *14*, 39.

(36) Belot, V.; Corriu, R. J. P.; Leclercq, D.; Mutin, P. H.; Vioux, A. *J. Polym. Sci., Polym. Chem.* **1992**, *30*, 613.

(37) Sorarù, G. D.; D'Andrea, G.; Campostrini, R.; Babonneau, F.; Mariotto, G. *J. Am. Ceram. Soc.* **1995**, *78*, 379.

Table 2. Density Measured by Pycnometry ($g \cdot cm^{-3}$) and Specific Surface Area, SSA, Measured According to the BET Method ($m^2 \cdot g^{-1}$)[a]

	T^HD^H 1		T^HD^H 2		T^HD^H 9	
pyrolysis parameters	density (g/cm^3)	ρ SSA ±5% (m^2/g)	density (g/cm^3)	ρ SSA ±5% (m^2/g)	density (g/cm^3)	ρ SSA ±5% (m^2/g)
gel	1.26 ± 0.02	46	1.34 ± 0.03	228	1.54 ± 0.01	673
1000 °C	2.45 ± 0.02	39	2.41 ± 0.01	108	2.24 ± 0.02	117
1200 °C	2.46 ± 0.01	32	2.43 ± 0.03	94	2.27 ± 0.01	0
1400 °C	2.48 ± 0.03	4.6	2.40 ± 0.01	0	2.27 ± 0.03	0
1500°C	2.49 ± 0.02	0	2.41 ± 0.02	0	2.17 ± 0.03	0

[a] The error for the density measurements is given as ± the standard deviation. The estimated error for the SSA measurements is ± 5%.

As suggested by several authors,[10,56] this reaction should proceed in the following steps:

$$SiO_2(s) + C(s) \rightarrow SiO(g) + CO(g) \quad (2)$$

$$SiO(g) + 2\,C(s) \rightarrow SiC(s) + CO(g) \quad (3)$$

In our samples with limited free-C contents, reaction 2 should be favored. In this case, gaseous silicon monoxide is an important intermediate species. Indeed, we did observe the condensation of SiO on the cold parts of the furnace. This escape of SiO has to be related to the low carbon content of our glasses, which does not allow for a complete conversion of SiO_2 into SiC. It is worth noting that this escape of SiO is not expected to change the O/Si molar ratio of the final material, as we observe experimentally.

The ceramic yields measured after each pyrolysis steps (with a holding time of 1 h) and those extracted from the TG curves are compared in Table 1. The trends are very similar even with nonidentical operative conditions. The ceramic yield at 1000 °C is high—around 90 wt % for the three systems. After pyrolysis at 1500 °C, it remains at this value for T^HD^H9, and slightly decreases to 80 wt % for T^HD^H1, as a consequence of a higher C content, responsible for partial carbothermal reduction to occur.

III.3. Density. The densities of the powdered samples are presented in Table 2 as a function of the pyrolysis temperature up to 1500 °C. The density of starting gels is markedly different depending on the composition: 1.26, 1.34, and 1.54 g/cm^3 for T^HD^H1, T^HD^H2, and T^HD^H9, respectively. It can be directly related to the degree of cross-linking of the siloxane network.[27] Upon pyrolysis at 1000 °C, T^HD^H1 and T^HD^H2 become denser than T^HD^H9. In the temperature range from 1000 to 1400 °C, T^HD^H1, T^HD^H2, and T^HD^H9 specimens maintain nearly constant density values (~2.47, ~2.42, and ~2.25 g/cm^3, respectively), which are consistent with the glass compositions. Increasing the temperature to 1500 °C induces a slight decrease of the density only for T^HD^H9 sample. This can be related to the onset of a decomposition process involving the formation of bubbles.[38]

III.4. N_2 Adsorption−Desorption Measurements. N_2 adsorption−desorption isotherms have been recorded as a function of the pyrolysis temperature. T^HD^H1, 2, and 9 show specific surface areas in gel state of 46, 228, and 673 m^2/g (±5%), respectively (Table 2). The cumulative pore volumes measured as a function of pore diameter (not shown here) show that most of the pores are in the range 100−300 Å for T^HD^H1 and below 100 Å for T^HD^H9. T^HD^H2 composition shows an intermediate behavior. After pyrolysis at 1000 °C the surface area is reduced to 38 m^2/g for T^HD^H1, 108 m^2/g for T^HD^H2, and 116 m^2/g for T^HD^H9. This phenomenon is mainly due to the elimination of a large part of the finer pores between 20 and 100 Å. It is accordingly more pronounced for T^HD^H9 and 2 than for T^HD^H1. At 1000 °C the average pore size is: ≈200 Å for T^HD^H1, ≈100 Å for T^HD^H2, and well below 100 Å for T^HD^H9. Larger pores are still present up to 1200 °C, except for T^HD^H9, where the increase in temperature leads to a linear decrease in surface area, almost vanishing at 1200 °C. For T^HD^H1 and 2, the temperature must be raised to 1400 °C to have a fully densified material.[38]

The different densification behavior (with pore elimination) of the SiCO glass powders observed at high temperatures (above 1000 °C) may be related either to their initial difference in pore size and amount or to the different viscosity of the silicon oxycarbide glasses which is known to depend on the SiCO composition.[39]

III.5. X-ray and Neutron Diffraction. The X-ray and neutron diffraction patterns collected on samples T^HD^H1, 2, and 9 after pyrolysis at 1000 °C are typical of amorphous phases. The corresponding reduced RDF Q(r) are reported in Figure 3 for the T^HD^H2 sample. The average interatomic distances, bond angles, and coor-

(38) Walter, S.; Soraru, G. D.; Brequel, H.; Enzo, S. *J. Eur. Ceram. Soc.* **2002**, *22*, 2389.
(39) Rouxel, T.; Massouras, G.; Sorarù, G. D. *J. Sol-Gel Sci. Technol.* **1999**, *14*, 83.
(40) Laffon, C.; Flank, A. M.; Lagarde, P.; Laridjani, M.; Hagege, R.; Orly, P.; Cotteret, J.; Dixmier, J.; Miquel, J. L.; Hommel, H.; Legrand, A. P. *J. Mater. Sci.* **1989**, *24*, 1503.
(41) Mozzi, R. L.; Warren, B. E. *J. Appl. Crystallogr.* **1969**, *2*, 164.
(42) Schaeffer, P. T. B. *Acta Crystallogr. Sect. B* **1969**, *25*, 477.
(43) Henderson, G. S.; Fleet, M. E.; Bancroft *J. Non-Cryst. Solids* **1984**, *68*, 333.
(44) Brequel, H.; Enzo, S.; Babonneau, F.; Radaelli, P. J. *Mater. Sci. Forum*. **2002**, *386−388*, 275.
(45) Sorarù, G. D.; D'Andrea, G.; Campostrini, R.; Babonneau, F.; Mariotto, G. *J. Am. Ceram. Soc.* **1995**, *78*, 379.
(46) Apperley, D.; Harris, R. K.; Marshall, G. L.; Thompson, D. P. *J. Am. Ceram. Soc.* **1991**, *74*, 777.
(47) Knight, D.; White, W. *J. Mater. Res.* **1989**, *4* (2), 385.
(48) Wang, Y.; Alsmeyer, D. C.; McCreery, R. L. *Chem. Mater.* **1990**, *2*, 557.
(49) Nemanich, R. J.; Solin, S. A. *Phys. Rev. B* **1979**, *20* (2), 392.
(50) Tuinstra, F.; Koenig, J. L. *J. Chem. Phys.* **1970**, *53* (2), 1126.
(51) Huong, P. V. *Ann. Chim. Fr.* **1983**, *8*, 73.
(52) Albers, P.; Prescher, G.; Seibold, K.; Ross, D. K.; Fillaux, F. *Carbon* **1996**, *34* (7), 903.
(53) Kroll, P. *J. Mater. Chem.* **2003**, *13* (7), 1657.
(54) Bois, L.; Maquet, J.; Babonneau, F.; Mutin, H.; Bahloul, D. *Chem. Mater.* **1994**, *6*, 796.
(55) Trassl, S.; Motz, G.; Rössler, E.; Ziegler, G. *J. Am. Ceram. Soc.* **2002**, *85*, 239.
(56) Belot, V.; Corriu, R. J. P.; Leclercq, D.; Mutin, P. H.; Vioux, A. *J. Non-Cryst. Solids* **1992**, *144*, 287.

Table 3. Average Interatomic Distances, Bond Angle, and Coordination Numbers Calculated from X-ray and Neutron RDF Calculations for the T^HD^H1, T^HD^H2, and T^HD^H9 Compositions Pyrolyzed at 1000 °C

	1st shell			2nd shell				Si−O−Si bond angle[a]
	X-ray	neutron		X-ray	neutron	X-ray	neutron	
T^HD^H1								
distance (Å)	1.67			2.69		3.06		
coord. number[b]	3.0			0.7		2.8		
T^HD^H2								
distance (Å)	1.66	1.62	1.88	2.61	2.64	3.05		140.6
coord. number[b]	2.9	3.1		0.6		3.7		
T^HD^H9								
distance (Å)	1.65	1.61	1.89	2.57	2.63	3.06	3.06	143.7
coord. number[b]	2.8			0.7		2.3		
atomic bonds involved	Si−O/Si−C	Si−O	Si−C	O−O (C−C)		Si−Si		

[a] Calculated from the first and the second main shell's position (neutron data). [b] Known to be underestimated by comparison with results obtained on a standard.

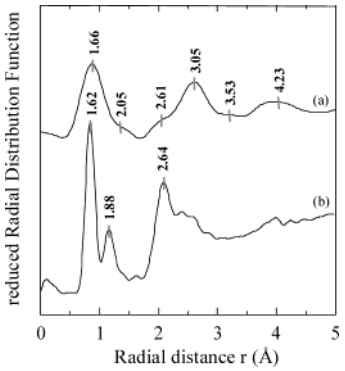

Figure 3. Reduced radial distribution functions calculated from the X-ray (a) and neutron (b) diffraction patterns for the T^HD^H2 sample pyrolyzed at 1000 °C.

dination numbers obtained for each composition are summarized in Table 3.

The bonding topology of a SiCO glass network is based on tetrahedral SiX_4 (X = O, C) units. Below 2 Å, we are thus expecting two characteristic bond distances due to Si−O and Si−C, if C has been successfully inserted in the silica network. Indeed, the RDF from neutron diffraction reveals two pair maxima, the first located at 1.61−1.62 Å and the second one at 1.88−1.89 Å, assigned, according to the literature,[40−43] to Si−O and Si−C bonds, respectively. On the other end, the RDF analysis from X-ray diffraction is able to evidence just one average distance located at 1.65−1.67 Å. The low resolution of X-ray patterns is essentially due to the limited Q-range available with Mo Kα, and to the low intensities of the high-Q features because of the quick drop-off of the X-rays scattering factors. The features at R > 2 Å correspond to O−O, Si−Si, and Si−2nd O pair distances. The value for the average bond angle O−Si−O (from the Si−1st O and O−O distances) is in good agreement with a tetrahedral geometry, around 109°. Average Si−O−Si bond angles ranging from 140° to 144° were calculated from the Si−1st O and Si−Si distances. These values are slightly smaller than the values found in the literature, 144 to 151°, for various forms of amorphous SiO_2.

The XRD patterns obtained from the glasses after heat-treatment at 1200, 1400, and 1500 °C are reported in Figure 4. The profile fitting and the Bragg peak positions of the expected phases of SiO_2, SiC, and Si are also shown with the experimental data. Some features related to SiC are present for samples treated at 1200 °C. The pure silicon phase is not present on the patterns of T^HD^H1 samples. In contrast, a very small quantity of silicon is detected in T^HD^H2 sample at 1400 °C and above, and for the T^HD^H9 sample whatever the temperature. An amorphous phase is present for every composition and at each pyrolysis temperature, which usually makes difficult the quantitative analysis by the Rietveld method. For modeling the amorphous phase we started from the structure of α-carnegieite (made up by SiO_4 tetrahedra sharing corners) described by Le Bail.[32] Because of the approximations involved, the quantitative phase analysis and crystallite size summarized in Table 4, should actually be regarded as semiquantitative. Note that the *β*-SiC (200) reflection is weak or absent in our XRD patterns. This could be due to the presence of stacking faults. Efforts to describe the SiC pattern with a combination of α- and *β*-SiC phases were less successful than a model with only *β*-SiC and stacking faults. The neutron diffraction patterns have also been recorded on the same samples, and the results are consistent with the X-ray diffraction analysis.[44] The decaying background of the patterns suggests that appreciable quantities of hydrogen atoms may still be present in the glass matrix up to the maximum pyrolysis temperature (1500 °C), as it will be further shown by ^1H NMR.

III.6. Transmission Electron Microscopy. The samples pyrolyzed at 1000 °C are completely amorphous as shown in the low-contrast featureless HRTEM images and their associated electron diffraction patterns (EDP), as for example shown in Figure 5a. Low-magnification images show the existence of a three-dimensional framework due to numerous micropores for T^HD^H1 (<600 Å) and T^HD^H2 (<200 Å), whereas no porosity was observed in the specimen T^HD^H9. Even after heat-treatment at 1200 °C, the samples T^HD^H1 and 2 are still very similar. EDP shows only diffuse halos of an amorphous phase with an additional feature at ∼2.51 Å, which could be attributed to nano-crystalline SiC. As compared to the 1000 °C samples, the specimens seem less porous with pore size about ∼400 Å. The conclusions on the evolution of the size and distribution of pores are only qualitative and perhaps not representative for the whole sample as the observations are very localized. However, there is an excellent correspondence between the direct TEM measurements and the surface

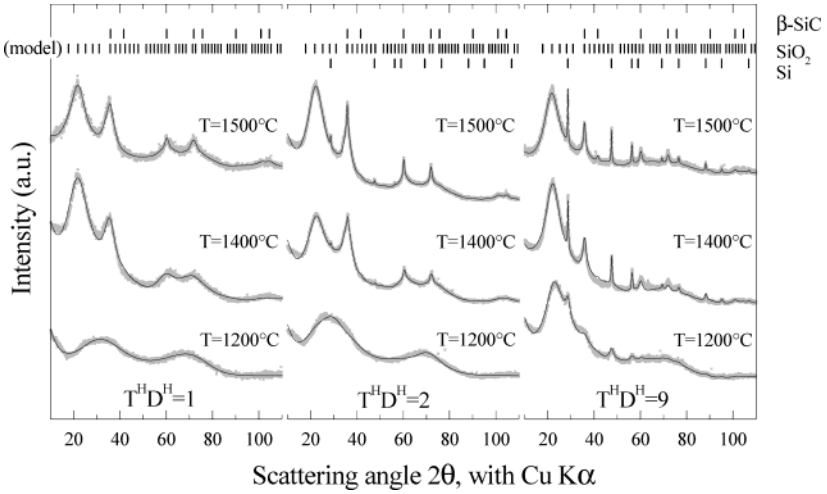

Figure 4. Experimental XRD patterns (grey dots) and Rietveld fit (full line) for the T^HD^H systems with various heat treatments.

Table 4. Quantitative Analysis and Crystallite Size of Phases after Rietveld Fit

Quantitative Analysis

	T^H/D^H1		T^H/D^H2			T^H/D^H9		
	SiC wt%	amorph. phase wt%	SiC wt%	Si wt%	amorph. phase wt%	SiC wt%	Si wt%	amorph. phase wt%
1200 °C		100	5	0	95	4	4	92
1400 °C	16	84	27	1	72	8	2	90
1500 °C	30	70	12	1	87	6	4	90

Crystal Size (nm)

	T^H/D^H1	T^H/D^H2		T^H/D^H9	
	SiC	SiC	Si	SiC	Si
1200 °C		1.0		1.5	2.5
1400 °C	**2.4**	1.5	31.0	3.0	14.5
1500°C	1.8	3.0	30.0	16	19.2

area values for all three specimens at each pyrolysis temperature. On the other hand, the specimen T^HD^H9 pyrolyzed at 1200 °C is similar to samples heat-treated at higher temperature (Figure 5b). Indeed, a homogeneous distribution of crystallites smaller than 300 Å embedded in a dense amorphous matrix was observed. In the corresponding EDP one can see the presence of many spots in all directions due to the diffraction of nonoriented grains, almost forming a ring pattern characteristic for polycrystalline samples. The distances measured on the EDP reveal the presence of both elemental silicon (at ∼3.1, 1.9, and 1.6 Å) and *β*-SiC inclusions (at ∼2.5, 1.5, and 1.3 Å). In addition, a diffuse ring at ∼4 Å was noticed corresponding to the presence of amorphous silica. Accordingly, the HRTEM images confirm the presence of either silicon and SiC crystallites with diameters up to 300 and 80 Å, respectively, at 1400 °C. After pyrolysis at 1500 °C both Si and SiC precipitates appear to grow reaching a maximum of 500 Å. They are still embedded in a matrix of amorphous silica, as identified by EDP.

The specimen T^HD^H2 heat-treated at 1200 and 1400 °C exhibits three different morphologies (Figure 5c). (i) Some grains are almost completely amorphous and contain rare features usually inferior at 60 Å in size, which are attributed to SiC precipitates. These grains can still be porous in the sample heat-treated at 1400 °C, whereas no porosity was observed after heat-treatment at 1500 °C. (ii) Other grains contain much more SiC precipitates distributed in a wide size range

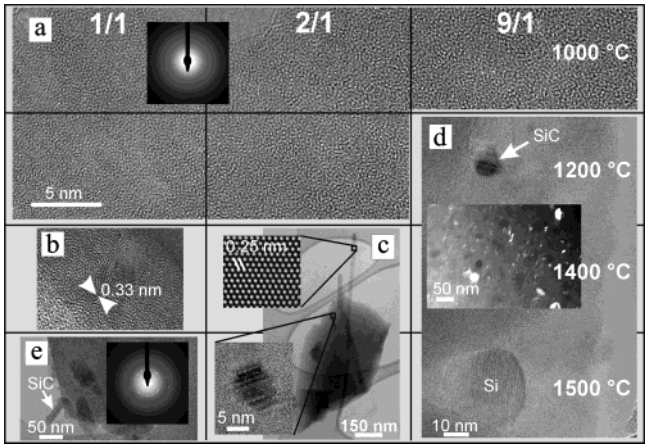

Figure 5. Table-like presentation of TEM results concerning the T^H/D^H samples which range from compositions 1:1 to 9:1. From top to bottom, the rows correspond to temperatures 1000, 1200, 1400, and 1500 °C. (a) HRTEM image of $T^HD^H = 9$ at 1000 °C with inset of the corresponding EDP. This amorphous-like image is characteristic for T^HD^H samples heat-treated at 1000 °C for all compositions and at 1200 °C for T^HD^H1 and 2. (b) HRTEM micrograph of the sample T^HD^H1 heated at 1400 °C, presenting some graphitic carbon features. (c) Low-magnification image characteristic for T^HD^H2 heated at 1400 and 1500 °C, showing the presence of both SiC fibers and SiC precipitates, whose HRTEM images are presented as insets. (d) HRTEM image characteristic for T^HD^H9 samples heated at 1200−1500 °C. HRTEM imaging and dark-field imaging (see inset) reveal the presence of numerous nanoprecipitates of either Si or SiC. (e) TEM image of the sample T^HD^H1 pyrolyzed at 1500 °C, and the corresponding EDP.

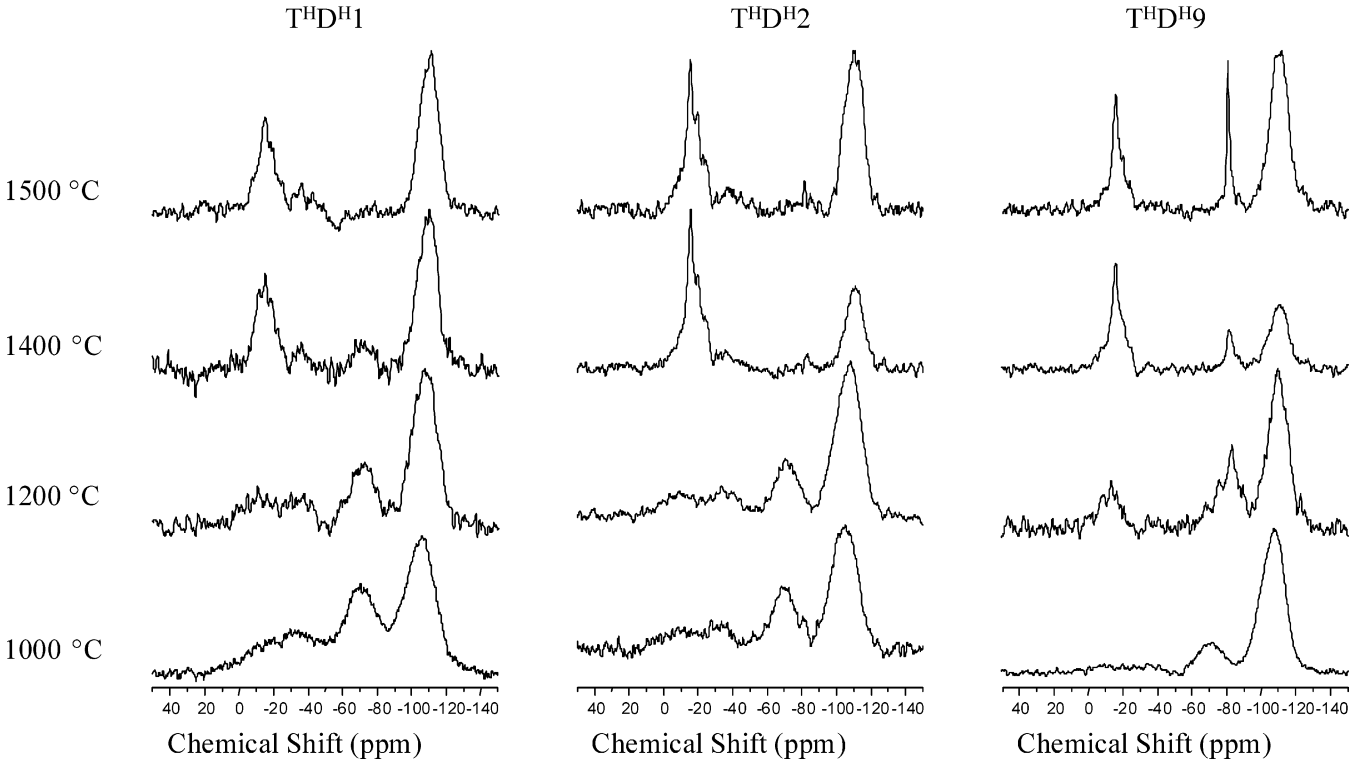

Figure 6. ^{29}Si MAS NMR spectra of T^HD^HX ($X = 1, 2, 9$) samples pyrolyzed at various temperatures (1500 °C spectrum measured with 15° pulses and 100-s recycle delay).

Table 5. Quantitative Analysis Determined for Si Species

sample	pyrolysis temp. (°C)	Si species (%)						SiCO composition	
		SiO_4	$SiCO_3$	SiC_2O_2	SiC_3O	SiC_4	Si	from NMR	from EA
T^HD^H1	1000	44	32	17	2	5	0	$SiC_{0.23}O_{1.54}$	$SiC_{0.39}O_{1.38}$
	1200	55	22	10	4	9	0	$SiC_{0.22}O_{1.55}$	$SiC_{0.38}O_{1.39}$
	1400	54	9	6	2	29	0	$SiC_{0.36}O_{1.28}$	$SiC_{0.35}O_{1.37}$
	1500	57	0	0	0	43	0	$SiC_{0.43}O_{1.14}$	$SiC_{0.33}O_{1.40}$
T^HD^H2	1000	56	25	10	3	6	0	$SiC_{0.19}O_{1.61}$	$SiC_{0.30}O_{1.49}$
	1200	59	20	10	4	7	0	$SiC_{0.20}O_{1.60}$	$SiC_{0.27}O_{1.49}$
	1400	38	0	0	0	62	0	$SiC_{0.62}O_{0.76}$	$SiC_{0.26}O_{1.41}$
	1500	37	0	0	0	57	6	$SiC_{0.57}O_{0.74}$	$SiC_{0.26}O_{1.42}$
T^HD^H9	1000	76	16	3	3	2	0	$SiC_{0.10}O_{1.80}$	$SiC_{0.14}O_{1.61}$
	1200	59	18	0	0	15	8	$SiC_{0.19}O_{1.45}$	$SiC_{0.12}O_{1.55}$
	1400	46	0	0	0	44	10	$SiC_{0.44}O_{0.92}$	$SiC_{0.13}O_{1.53}$
	1500	33	0	0	0	54	13	$SiC_{0.54}O_{0.66}$	$SiC_{0.11}O_{1.57}$

(50−1000 Å). And finally, (iii) fibers of crystalline SiC long enough to prolong outside the SiCO particles. The combination of EDP and HRTEM imaging reveals that these fibers are essentially composed of α-SiC with rather few defects, while the smaller precipitates are nanocrystalline β-SiC. Increasing the pyrolysis temperature to 1400 °C for sample T^HD^H1, it is possible to see some rare features corresponding to graphitic carbon (d spacing distance ∼3.35 Å; Figure 5d) embedded in an amorphous matrix. The corresponding EDP presents only broad peaks due to the presence of SiC in a nanocrystalline state (broad peaks at ∼2.51, ∼1.54, and ∼1.32 Å). In addition, some SiC crystallites up to 1000 Å were found in the same sample heat-treated at 1500 °C but no graphitic features were observed. However, similar to the 1400 °C sample, the corresponding EDP contains three broad peaks due to "disordered" SiC plus some weak but definite spots originating from the SiC crystallites (Figure 5e).

III.7. MAS NMR. The characterization by ^{29}Si MAS NMR of the three T^HD^H compositions are illustrated in Figure 6. Measurements of spin−lattice relaxation times were carried out on samples pyrolyzed at 1000 °C to ensure proper quantitative analysis of the spectra. They vary from 15 to 20 s, depending on the type of Si units. At 1000 °C, the three spectra typically represent that of a silicon oxycarbide glass containing a distribution of SiC_xO_{4-x} units (where $0 \le x \le 4$).[45] Depending on the composition of the starting gels, these glasses exhibit various amounts of the following units: SiO_4 (∼107 ppm), $SiCO_3$ (∼72 ppm), SiC_2O_2 (∼34 ppm), SiC_3O (∼1 ppm), and SiC_4 (∼16 ppm). The spectra have been simulated (Table 5), but the large overlap of the signals due to SiC_2O_2, SiC_3O, and SiC_4 units may have led to some uncertainties in the quantitative analysis. However, comparison between samples can be made to extract general trends. The stoichiometries of the various oxycarbide phases at 1000 °C were estimated by assuming that the C atoms in these phases are bonded to 4 Si atoms. This does not take into account the presence of residual hydrogen found by chemical analysis for T^HD^H1. The following values were found: $SiC_{0.23}O_{1.54}$ for T^HD^H1, $SiC_{0.20}O_{1.60}$ for T^HD^H2, and $SiC_{0.10}O_{1.80}$ for T^HD^H9. At 1000 °C, the T^HD^H1 and

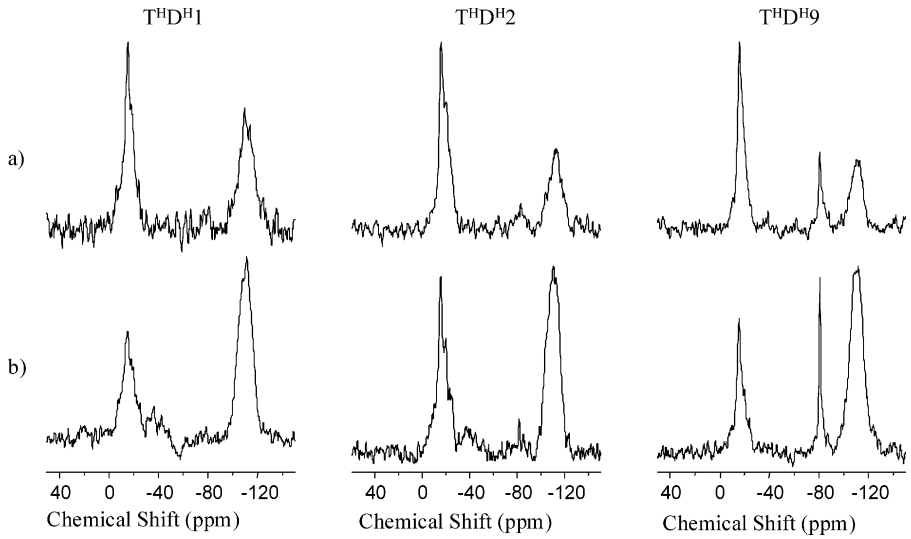

Figure 7. ^{29}Si MAS NMR spectra of T^HD^HX (X = 1, 2, 9) samples pyrolyzed at 1500 °C: (a) 90° pulses and 150-s recycle delay; and (b) 15° pulses and 100-s recycle delay.

T^HD^H2 glasses are thus composed of a silicon oxycarbide phase with similar C content, while the T^HD^H9 glass has a significantly lower level of oxycarbide units due to the low D^H amount in the starting gel. The line widths for the Si-species are broad and equal within each composition. This is characteristic of amorphous networks in which exist a random distribution of environments. The amounts of free carbon in the glasses can be estimated by comparison between the EA and NMR results following a method already reported in the literature[45] (Table 5). At 1000 °C, the free C to silicon molar ratio was deduced as 0.16, 0.11, and 0.04 C_{free}/Si for T^HD^H1, T^HD^H2, and T^HD^H9, respectively. These values should be taken with great care, if one considers the uncertainties on the NMR and elemental analyses; however, they show clearly the expected trend with a reduction of the free C content when going from T^HD^H1, to T^HD^H2, and T^HD^H9.

On increasing the pyrolysis temperature, the NMR data show a redistribution of bonds within the system as seen by a decrease in SiC_xO_{4-x} (where $1 \leq x \leq 3$) with respect to SiC_4 and SiO_4 units. For T^HD^H1, the evolution is gradual starting from 1000 °C and going up to 1500 °C. T^HD^H2 exhibits a different peak evolution. Here, phase separation is no longer gradual and occurs rapidly between the pyrolysis temperatures 1200 and 1400 °C. Additionally, at 1500 °C a small peak emerges at −82 ppm that is due to elemental silicon. For T^HD^H9 the phase transformation is similar to that of T^HD^H2 in that it is rapid after 1200 °C. The formation of elemental silicon is also seen in larger quantities and starting at lower temperatures. At 1200 °C, a sharper peak at −83 ppm can be seen as partial contribution toward a larger asymmetric peak also containing $SiCO_3$ units (−77 ppm). Once the phase separation between silicon carbide and silica has been almost completed (at 1500 °C for T^HD^H1 and 1400 °C for T^HD^H2 and 9), one can observe a peak-narrowing for the resonance peaks due to SiC indicating a better crystalline state. It is even possible to distinguish several peaks at −15, −20, and −24 ppm, which are due to the presence of crystalline β-SiC, with some well-defined sites related to α-polytypes.[46]

The compositions of the silicon oxycarbide phases detected by ^{29}Si MAS NMR experiments are reported in Table 5, and compared with the EA results. The total carbon content by EA. should be equal to or greater than that deduced by NMR, which is not always the case above 1000 °C. The C content within the SiC-rich phase seems very much overestimated in the NMR spectra particularly at higher temperatures and for the T^HD^H9 composition. This suggests that, for these samples, the experimental parameters that were chosen according to the T_1 measurements done on the 1000 °C samples (90° pulses with 100−150-s recycle delays) were not appropriate for a quantitative detection of the Si sites, suggesting an increase of the T_1 values with temperature. Indeed, spectra of the 1500 °C samples recorded with shorter pulse width (Figure 7) clearly show a significant enhancement of the signals due to the Si and SiO_2-rich phases. One should thus be very careful to perform quantitative analysis of the ^{29}Si MAS NMR spectra recorded on this type of samples.

High spinning rate ^{1}H MAS NMR spectra were recorded on the four pyrolyzed specimens of the T^HD^H1 composition (Figure 8). For each annealing temperature, the final Fourier transform which is shown was obtained by subtraction of the empty rotor signal (probably mainly due to the presence of aromatic protons into the Vespel caps of the rotor) to the experimental recording (see inset for the 1000 °C spectrum). This mathematical treatment of the signal could nevertheless generate some artifact on the spectrum, which appears in the domain of aromatic protons, especially for low signal/noise ratios.

The general trend of the spectra is a decrease of the signal intensity with increasing temperature, due to the drastic diminution of proton content in the material from 1000C to 1500 °C. At 1000 °C, the presence of residual hydrogen found by chemical analysis for the T^HD^H1 system (∼1 wt %; Cf. Table 1) yields to a signal composed of two peaks located at 3.5 and 0.7 ppm, as well as a shoulder at ∼7 ppm, referred to TMS. The peak at 0.7 ppm is related to protons linked to sp^3 carbon atoms ($(Si-)_3CH$ type). The attribution of the first peak is related to the formation at high temperature of some

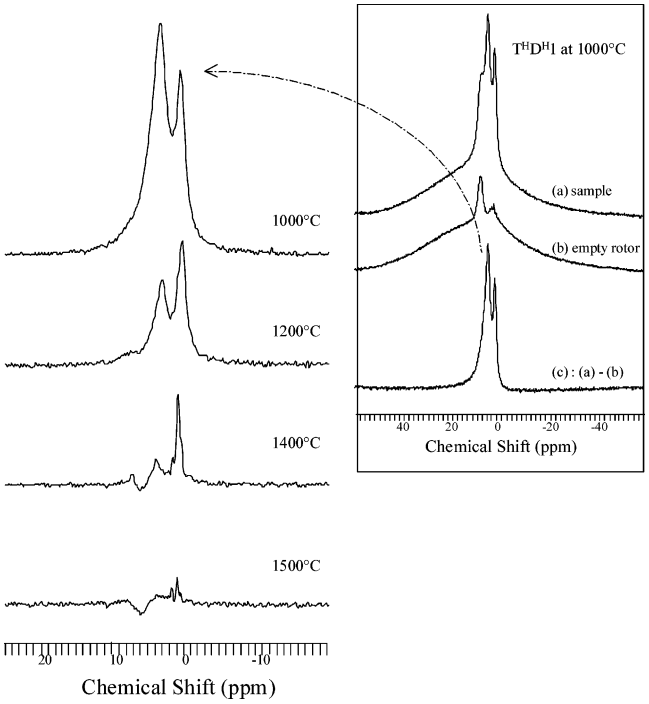

Figure 8. ^{1}H High-speed MAS NMR spectra of the sample T^HD^H1 pyrolyzed at various temperatures, and description of the calculation method for the 1000 °C spectrum obtained by subtraction of the empty rotor signal to the experimental recording (in inset).

hydroxyl (≡Si−O*H* and probably also H−O*H* of adsorbed water) groups.

The last peak at ∼7 ppm could be attributed to aromatic protons chemically bound to the sp^2 carbon atoms of the free-C phase present in the material as a graphite-like structure evidenced by INS and TEM.

Even if these ^{1}H NMR experiments were not recorded under quantitative conditions because there was no calibration by an internal standard, our study could nevertheless give some interesting features about the evolution of the two major peaks intensity ratio when temperature rises. Actually, we can note a drastic breakdown of the −O*H* peak between 1000 and 1400 °C, which can be related to the decrease of the specific surface area observed by N_2 sorption because of material densification. At 1500 °C, the signal is extremely weak, indicating that only traces of residual protons are still present in the material at this ultimate temperature, as was also concluded by neutron diffraction. So we can see how ^{1}H NMR is a powerful tool for studying materials containing various kinds of protons in small quantities, which, in the present case, allows us to follow the proton signal until 1500 °C, whereas the detection limits of elemental analysis are reached at 1200 °C.

III.8. Vibrational Spectroscopies. Raman spectra of the three sets of specimens after the different pyrolysis temperatures are shown in Figure 9. Only fluorescence is observed in the spectra of the glasses, for all the samples treated at 1200 °C, and for the specimens T^HD^H1 and 2 pyrolyzed at 1400 °C. This phenomenon may be associated with defects present in these samples due to, for example, porosity and radical formation. Indeed, an ESR study (not shown here) shows the formation of radicals during pyrolysis, with an optimum amount around 1200 °C which strongly decreases by 1500 °C. The sample T^HD^H1 treated at 1500 °C shows two clear bands at 1349 and 1601 cm^{-1}, respectively assigned to the D and G bands of glassy carbon.[47] The G band has been assigned to the predicted E_{2g} mode of graphite. The D band (for disorder) has attracted considerable debate in the literature. It does not appear in large-grain single crystals but does appear in well-crystallized graphites with small particle sizes. Most of the reports concur that this band is related to structural disorder, but there is no clear consensus on its origin.[48−50] Using a correlation found in the literature,[47] the intensity ratio between these two bands allows us to estimate the average carbon domain size in this sample to be about 25 Å. For T^HD^H2 heat-treated at 1500 °C, a distinct peak at ca. 517 cm^{-1} is present, clearly due to the elemental silicon.[51] As for T^HD^H9, this characteristic band of elemental silicon starts appearing at a lower temperature of 1400 °C and increases in intensity after heat treatment at 1500 °C.

For the inelastic neutron scattering (INS) spectra (Figure 10) the selection rules similar to IR and Raman spectroscopies do not apply. All vibrations are thus active. However, the intensity of a normal mode is solely determined by the inelastic neutron scattering cross-section and the amplitude of vibration of the atoms involved in the normal mode. Because hydrogen has a cross section much larger than that for any other element, and its amplitude of motion is also large due to its very low mass, motions involving hydrogen tend to dominate the spectra. The spectral changes observed

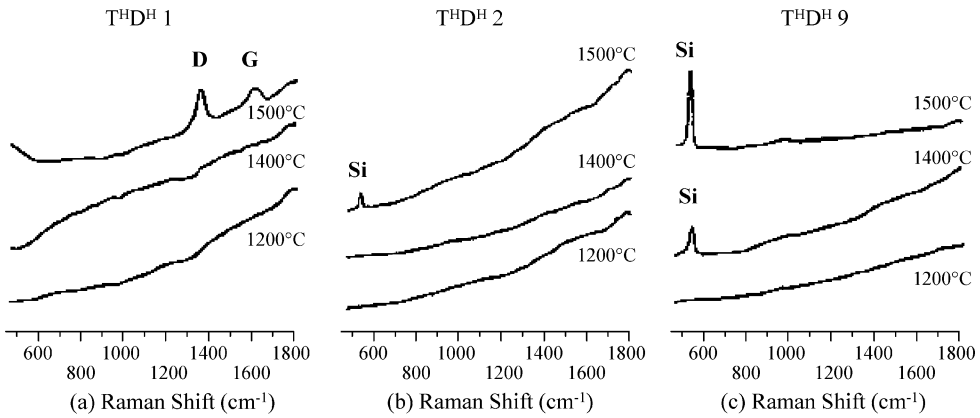

Figure 9. Raman spectra of the T^HD^H1 (a), T^HD^H2 (b) and T^HD^H9 (c) samples pyrolyzed at various temperatures (laser lines are 441.6 nm from He−Cd laser for T^HD^H2 and 9, and 514.5 nm from Ar^+ laser for T^HD^H1).

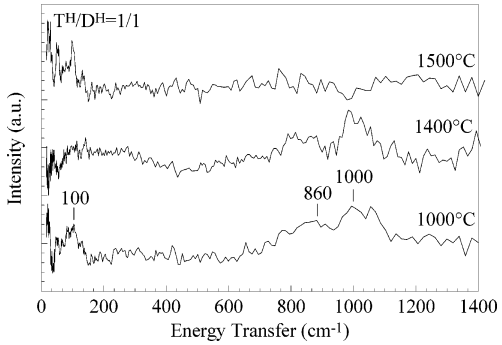

Figure 10. INS spectra of the T^HD^H1 sample pyrolyzed at various temperatures.

with increase in sample annealing temperature clearly show the disappearance of different hydrogenous species such as CH_3 and CH_2 by about 600 °C. These disappearances are followed, at 1000 °C, by the appearance of two weak broad bands at about 860 and 1000 cm^{-1} which remain until 1400 °C (Figure 10). According to Fillaux et al.,[52] these broad bands correspond to vibrations of protons chemically bound to heavy atoms such as C, O, S, etc. Another observation of interest in the INS is the appearance of a band at ca. 100 cm^{-1} in the sample pyrolyzed at 1000 °C which can be assigned to lattice modes of a graphite-like structure in agreement with published data on carbon.[52] The observed intensity is likely to be due to hydrogens associated with the free carbon. Therefore, the sharp peak remaining even at 1500 °C suggests the presence of trace amounts of hydrogen, this even after pyrolysis at such high temperature. Fillaux et al.[52] have identified features in the INS spectra of many such systems at ca. 880 and 1170 cm^{-1} with loosely bound hydrogens and have assigned these to C−H bonds in a distribution of anharmonic potential wells. The matrix of silicon oxycarbide glasses is different from that of any system studied before, and the shifts in frequency of these broad features when compared to protons in other matrixes, such as pure carbon, are therefore not surprising. These features disappear in the spectrum of the 1500 °C sample, showing significant decrease in the residual hydrogen content, as also shown by ^1H solid-state NMR at this stage of pyrolysis.

The vibrational spectroscopic technique of choice for the detection of silicon carbide is infrared spectroscopy. As a matter of fact, a clear peak at 795 cm^{-1} observed in the IR spectra for T^HD^H2 (1400 and 1500 °C) and T^HD^H1 (1500 °C) is attributed to Si−C bond stretching; its sharpness indicating "topological" crystallinity. However, this band seems to be broadened and shifted to ca. 806 cm^{-1} for the 1400 and 1500 °C T^HD^H9 pyrolyzed samples. This effect may be related to the crystallite size of the silicon carbide particles.

IV. Discussion

IV.1. Glasses at 1000 °C. The wide range of collected structural data allows us to get a good description of the short-range order as well as the microstructure of these SiCO glasses. First, elemental analysis has confirmed that the strategy that was chosen to prepare glasses close to the stoichiometric $SiC_xO_{2(1-x)}$ composition, but with different carbon contents, is successful. TEM observations (supported by electron diffraction patterns) show the completely amorphous nature of these glasses, i.e., the absence of any long-range ordered structure. However, combination of NMR, X-ray, and Neutron scattering experiments allows us to get a good description of the glass short-range order.

The compositions of the silicon oxycarbide phase were clearly identified by ^{29}Si MAS NMR experiments. This technique has already been used to characterize a large number of SiCO glasses because it gives a direct quantitative evidence for the existence of various SiC_xO_{4-x} units. Quantification of these mixed SiC_xO_{4-x} units was even achieved, however with a certain level of uncertainty due to some peak overlap and rather low signal/noise ratio. The silicon oxycarbide phases in T^HD^H1 and T^HD^H2 have rather similar composition (C/Si = 0.23 and 0.20, respectively) whereas the C content is lower (C/Si = 0.10) in T^HD^H9. It has to be pointed out, however, that in the present work spin−lattice relaxation times were measured to optimize the conditions for quantitative analysis. The distributions of Si sites in the various samples have been compared with the values expected for an ideal random alternating network based on structural models proposed by Kroll[53] using density functionnal theory, for stoichiometric amorphous SiCO glasses with various compositions. He found that a perfect random network structure of the glassy phase appears valid for low C concentrations (C/Si < 0.33). Our NMR results compare reasonably well with such a model. Indeed, similar observation was already done by Mutin[13] who found that oxycarbide networks over a large range of stoichiometries ($0.1 \leq C/Si \leq 0.4$) can be described as a random distribution of Si−O and Si−C bonds.

The short-range order of these glassy samples has also been investigated for the first time through the analysis of the radial distribution functions (RDF) obtained from the Fourier analysis of X-ray and neutron structure factors. In all three specimens, the neutron diffraction data clearly show two distinct contributions at 1.61−1.62 Å and 1.88−1.89 Å for the first coordination shell assigned to Si−O and Si−C atomic pairs, respectively, in agreement with the presence of mixed SiC_xO_{4-x} units. The average Si−O−Si bond angle values from 140 to 144° are smaller than that found for amorphous silica and decrease with the inserted C amount.

One can see here how RDF and ^{29}Si NMR results are complementary: NMR can distinguish the various tetrahedral SiC_xO_{4-x} environments, but is not sensitive to their connectivity. RDF provides an average description for a Si tetrahedron, but with distances to the first as well as the second neighboring atoms, which can give some ideas about bond angles and thus connectivity. The distribution of bond distances and bond angles that Kroll[53] calculated are in good agreement with the average values that we have extracted from our experiments. This modeling shows that the distribution of the bending angle at O shifts toward lower angle values with the increase in C content, as does our experimental data.

Besides a silicon oxycarbide phase, these SiCO glasses may contain a free carbon phase. Raman scattering is very sensitive to the presence of free carbon. Unfortunately, in samples heat-treated at 1000 °C, a large

fluorescence background prevents the detection of any signals. This seems characteristic for these chemically derived glasses[45] and may be due to defects such as radicals, which form during the polymer-to-glass transformation as evidenced by ESR.[54] ^{13}C NMR should be an ideal technique to detect the C-containing phases,[55] but the low sensitivity of this nucleus combined with relatively long T_1 relaxation times prevented us from detecting any signal in a reasonable time in these low C content phases. The use of ^{1}H-^{13}C cross-polarization technique can overcome these problems, but leads to a selective detection of C sites with protons in their close environment. The low H content in these glasses will thus lead to the detection of a minority of C sites. An indirect evidence for the presence of free carbon indeed comes from the comparison between the ^{29}Si NMR and EA results, as already mentioned in Section III.7 (see also Table 5). The possibility of the existence of some covalent bonds between the free C phase and the oxycarbide phase cannot be excluded. One should emphasize, however, that such bondings should cause a shift in the ^{29}Si NMR peak position of the corresponding Si units (−65 ppm for a CH_3SiO_3 unit versus −80 ppm for a $PhSiO_3$ unit). But the large distribution of Si sites, which leads to extensive broadening of the resonance peaks, prevent any definitive conclusion regarding the existence of these bonds.

Protons can be detected either by ^{1}H NMR and INS. The first technique is a specific and powerful tool for distinguishing aliphatic protons linked to sp^3 carbon atoms from the hydroxyls, with eventually the possibility for some protons to be linked to sp^2 carbon atoms (in a minor amount). From the INS spectra extended over a wide energetic range and used for the first time in these systems, the existence of C−H modes related to graphene rings[52] in the glasses pyrolyzed at 1000 °C has been suggested. This is an unprecedented result that needs to be exploited further in other systems if an extensive knowledge of these materials is desired.

Specific surface area values of the glasses are still significant after pyrolysis at 1000 °C and are the result of the profound chemical and physical transformations occurring during pyrolysis, as well as the porosity level and pore size distribution of the starting gels. Pycnometric measurements performed on the three glasses show that their skeletal density is significantly larger than that of pure silica (2.25 g/cm^3) beyond the experimental uncertainty. In particular, the values for T^HD^H1 and 2 (∼2.5 g/cm^3) are very close and quite distinct from that of T^HD^H9 (∼2.3 g/cm^3). This suggests the occurrence of a more efficiently packed Si−C−O network in the former two C-rich specimens. This trend is similar to that predicted by Kroll,[53] and is also in agreement with the lower Si−O−Si bonding angle as previously discussed. Finally, pore size distribution obtained from the desorption part of the N_2 adsorption/desorption experiments[38] is in good agreement with TEM direct observations.

IV.2. Glasses Pyrolyzed above 1000 °C. According to the chemical compositions of the three glasses (Figure 1), different high temperature behaviors are expected. T^HD^H2 should form a binary mixture of xSiC and $(1 - x)SiO_2$, whereas the T^HD^H1 and T^HD^H9 samples should lead to ternary mixtures with additional C and Si phases, respectively. The expected amount of SiC should increase from T^HD^H9 to T^HD^H1 compositions.

TEM analysis confirms (with direct images) that atomic rearrangements of the glassy network are involved during pyrolysis. Crystallization of SiC occurred for all compositions with different growth rates that will be discussed later. Formation of free carbon has only been evidenced in the T^HD^H1 sample at high temperatures (> 1400 °C) by TEM and also by Raman scattering (domain size around 2.5 nm). However, the difficulty of detecting the presence of this phase by Raman, which is usually quite sensitive to C phases, prove that it is present in low quantity (<2 wt % from EA). In T^HD^H9, instead, the formation of Si crystallites (5 wt % from EA) could be detected by HR-TEM, X-ray and neutron diffractions, and ^{29}Si MAS NMR, as well as Raman scattering.

The high-temperature structural evolution of the amorphous phase toward the thermodynamically stable phases has been followed by several techniques sensitive either to local order (^{29}Si MAS NMR) or to long-range order (X-ray and neutron diffractions, HR-TEM).

There is a good correlation in the qualitative evolution versus pyrolysis temperature of the XRD patterns, ^{29}Si MAS NMR spectra, and HR-TEM images, especially with respect to the onset of crystallization and to the crystal size of Si and SiC. The Rietveld method used to quantitatively analyze the XRD data has been applied, for the first time in these glasses, to extract the amounts of the various phases and crystallite sizes (Table 4). These data should actually be regarded as semiquantitative considering the nature of approximations employed for our numerical approach.

The onset for crystallization of β-SiC in SiCO glasses seems dependent on the amount of carbon. Indeed, for the T^HD^H2 and 9 samples already at 1200 °C, ∼5 wt % of crystalline phase can be detected, whereas for the T^HD^H1 glass, pyrolysis temperature must be increased up to 1400 °C to promote crystallization, in good agreement with the TEM results. Other useful information can be obtained from the evolution of the crystal size with the pyrolysis temperature (Table 4). The composition which shows the highest crystal size value at all temperatures is the one with the lowest C content, i.e., the T^HD^H9. This glass is also the one that displays the strongest crystal growth effect with the annealing temperature, especially between 1400 and 1500 °C (from 3 to 16 nm). On the other hand, T^HD^H1 and 2 show, at each temperature, very small crystal size values (below 3 nm). All these data suggest that the crystallization of silicon carbide in SiCO glasses is slower for compositions rich in carbon. Indeed, carbon bonded to silicon in the oxycarbide network can delay the crystallization process: the presence of Si−C bonds can increase viscosity[5] and decrease short-range diffusion, while the presence of turbostratic carbon can act as a physical barrier between the SiC nuclei and the amorphous SiCO phase. Finally, it should be noticed that the strong crystal growth effect observed for the T^HD^H9 sample between 1400 and 1500 °C occurs without a corresponding definite increase in crystalline SiC wt %, and therefore should be regarded more as an Ostwald ripening process than a crystal growth stage.

Another interesting point to be noticed is the high stability of the silica phase in these glasses. Indeed, after the occurrence, in the temperature range 1200−1400 °C, of the phase separation into an amorphous-SiO_2/β-SiC nanocomposite material, the temperature can be increased even further, up to 1500 °C, without crystallization of the silica glass. This effect may be related to the presence of residual Si−C bonds in the silica structure which can hinder the rearrangement toward crystalline silica. Another possibility could be that silica does not form a continuous matrix but is present in a cluster of which the dimensions (1−2 nm) are too small to nucleate cristobalite.

The BET surface areas of the three glasses reduced to 0 at 1400 °C for T^HD^H1 and 2, and at a lower temperature (at 1200 °C) for the T^HD^H9 specimen. Rouxel et al.[5] have reported an increase in viscosity of 2 orders of magnitude for the same T^H/D^H2 silicon oxycarbide with respect to conventional SiO_2 glass. This result has been related to the presence of tetracoordinated C atoms which strengthen the silica network. Thus, the pore elimination seems to be controlled by viscous sintering in the glass transition temperature range, which is expected to be between 1300 and 1350 °C for the T^H/D^H1 and 2 compositions, and at lower temperatures for the T^H/D^H9 glass that has a lower carbon content.

The TGA data show no substantial changes in the char yield of each composition in the temperature range 1000−1300 °C, and a decrease at higher temperatures (excluding T^H/D^H9), which is accompanied by a lowering of C/Si ratio and by a modest lowering of the O/Si ratio. This behavior may be related to the observed evolution of CO (detected by MS) and possibly SiO gases (already reported in the literature[10,56]).

V. Conclusions (Summary)

In this study the structural characterization of three sol−gel-derived SiCO glasses with composition close to the stoichiometric one, $SiC_xO_{2(1-x)}$, but with different carbon contents, has been performed. Quantitative information concerning the structure of glasses before and after annealing at high temperature (1500 °C) was collected with a wide gamut of techniques (some of them used for the first time in this field) with the aim of probing the (i) short-range order and chemical composition (^{29}Si, ^{1}H MAS NMR, RDF derived from X-ray and neutron scattering, inelastic neutron scattering, FT-IR, and elemental analysis) and (ii) long-range order (X-ray and neutron diffraction) and microstructural features (HR-TEM combined with electron diffraction, Raman, porosity, and surface area measurements).

The main results can be summarized as follows. For SiCO glasses pyrolyzed at 1000 °C: (i) TEM observations (supported by X-ray and electron diffraction patterns) show the completely amorphous nature of the glasses, independently from their C content. (ii) ^{29}Si MAS NMR experiments give direct quantitative evidence for the existence of various SiC_xO_{4-x} units. The distributions of Si sites in the various samples compare well with the values expected for an ideal random alternating network, in agreement with the observation of Mutin[13] and the calculations of Kroll.[53] (iii) High-spinning-rate ^{1}H MAS NMR allows the detection of small amounts of protons present in the material and distinction between their different kinds: protons linked to C-sp^3 atoms on one hand and protons of hydroxyl groups on the other hand. (iv) In all three specimens the neutron diffraction data clearly show two distinct contributions at 1.61−1.62 and 1.88−1.89 Å for the first coordination shell assigned to Si−O and Si−C atomic pairs, respectively, in agreement with the presence of mixed SiC_xO_{4-x} units. The average Si−O−Si bond angle values from 140 to 144° are smaller than that found for amorphous silica, decrease with the inserted C amount, and agree with the structural models proposed by Kroll[40] using density functionnal theory for stoichiometric amorphous SiOC glasses with various compositions. (v) Raman spectra show a large fluorescence background which prevents the detection of any signals. (vi) INS spectra suggest the existence of C−H modes related to graphene rings in the glasses pyrolyzed at 1000 °C. (vii) Skeletal density of glasses is significantly larger than that of pure silica (2.25 g/cm^3) suggesting the occurrence of a more efficiently packed Si−C−O network. This result is in agreement with that predicted by Kroll[40] and it is also in agreement with the lower Si−O−Si bonding angle as previously discussed.

For SiCO glasses pyrolyzed at 1200−1500 °C, the following results were obtained: (i) On increasing the pyrolysis temperature ^{29}Si MAS NMR data show a redistribution of bonds within the system as seen by a decrease in SiC_xO_{4-x} (where $1 < x < 3$) with respect to SiC_4 and SiO_4 units. This evolution occurs at lower temperature for the samples with lower amount of C and shifts to higher temperature for SiCO glasses with high C content. (ii) The compositions of the silicon oxycarbide phases detected by ^{29}Si MAS NMR experiments seem to overestimate the C content within the SiC-rich phase particularly at higher temperatures and for the T^HD^H9 composition. One should thus be very careful to perform quantitative analysis of the ^{29}Si MAS NMR spectra recorded on this type of samples. (iii) There is a good correlation in the qualitative evolution versus pyrolysis temperature of the XRD patterns, ^{29}Si MAS NMR spectra, and HR-TEM images, especially with the respect to the onset of crystallization and to the crystal size of Si and SiC. (iv) The onset for crystallization of β-SiC in SiCO glasses seems dependent on the amount of carbon. For the glasses with lower C content already at 1200 °C ∼5 wt % of crystalline phase can be detected, whereas for the T^HD^H1 glass the pyrolysis temperature must be increased up to 1400 °C to promote crystallization. (v) The crystal growth rate of both SiC and Si seems inversely dependent from the C content. (vi) Evidence for the presence of free C has been obtained on the high C sample at 1400−1500 °C both from HR TEM and Raman experiments. (vii) From a microstructural point of view, increasing the temperature leads to a complete reduction of the porosity through a viscous sintering mechanism. The temperature at which the glasses become dense increases with the amount of C (1200 °C for T^HD^H9 and 1400 °C for T^HD^H2 and 1). This effect is related to the increase of glass viscosity with the C content in the oxycarbide network.

Acknowledgment. We thank the European Commission who supported this work through the Training

and Mobility of Researchers (TMR) Program (Contract FMRX-C.T.98-0161). Thanks to Laboratoire de Chimie de la Matière Condensée of Université Pierre & Marie Curie (Paris VI, FR) for hospitality and resource availability to some of the authors.
CM049847A